Study of Al-Alloy Foam Compressive Behavior Based on Instrumented Sharp Indentation Technology

Amkee Kim*
*Division of Mechanical and Automotive Engineering, Kongju National University,
Shinkwan-dong 182, Kongju, Chungnam 314-701, Korea*
Kazi Tunvir
*Division of Mechanical and Automotive Engineering, Kongju National University,
Shinkwan-dong 182, Kongju, Chungnam 314-701, Korea*

The stress-strain relation of aluminum (Al) alloy foam cell wall was evaluated by the instrumented sharp indentation method. The indentation in a few micron ranges was performed on the cell wall of Al-alloy foam having a composition of Al-3wt.%Si-2wt.%Cu-2wt.%Mg as well as its precursor (material prior to foaming). To extract the stress-strain relation in terms of yield stress σ_y, strain hardening exponent n and elastic modulus E, the closed-form dimensionless relationships between load-indentation depth curve and elasto-plastic property were used. The tensile properties of precursor material of Al-alloy foam were also measured independently by uni-axial tensile test. In order to verify the validity of the extracted stress-strain relation, it was compared with the results of tensile test and finite element (FE) analysis. A modified cubic-spherical lattice model was proposed to analyze the compressive behavior of the Al-alloy foam. The material parameters extracted by the instrumented nanoindentation method allowed the model to predict the compressive behavior of the Al-alloy foam accurately.

Key Words : Nanoindentation, Computer Simulation, Aluminum Foam, Constitutive Relation, Deformation, Mechanical Properties

Nomenclature

A_m: Projected contact area of indenter at maximum load [m²]
C : Loading curvature [N/m²]
c^* : Constant
E : Elastic modulus of indented material [GPa]
E_{in}: Elastic modulus of indenter material [GPa]
E^* : Effective elastic modulus [GPa]
h : Depth of indentation [m]
h_m : Maximum indentation depth [m]
K : Strength coefficient
n : Strain hardening exponent

P : Indentation load [N]
H_{ave}: Hardness of indented material
P_m : Maximum indentation load [N]
P_u : Unloading load [N]
ε : Total effective strain
ε_p : Nonlinear plastic strain
ε_r : Representative strain
ε_y : Linear elastic strain at yield
σ_r : Representative stress [MPa]
σ_y : Yield stress [MPa]
υ : Poisson's ratio of indented material
υ_i : Poisson's ratio of indenter material

* Corresponding Author,
  E-mail : amkee@kongju.ac.kr
  TEL : +82-41-850-8616; **FAX** : +82-41-854-1449
  Division of Mechanical and Automotive Engineering,
  Kongju National University, Shinkwan-dong 182, Kongju,
  Chungnam 314-701, Korea. (Manuscript **Received** November 18, 2005; **Revised** March 29, 2006)

1. Introduction

Metal foams have gained a growing research interest in automotive and aerospace industries due to their ultra-light weight and other attractive mechanical characteristics such as high specific

strength, excellent impact energy absorption, high damping capacity and good sound absorption capability. In particular, their crashworthiness in structural applications is mainly due to their plastic deformation characteristics to absorb impact energy in a controlled manner. Since the industrial applications of Al-alloy foams in various engineering fields depend on the availability of numerical tools that can reliably account various aspects of foams, a great exertion has been accomplished so far toward the development and use of numerical models for mechanical behavior analysis of Al-alloy foams. In this case, the stress-strain relation of cell wall material as an input parameter is very important for the accurate result. Nevertheless, most of the previous works (Santosa and Wierzbicki, 1998 ; Simone and Gibson, 1997 ; Overaker et al., 1998 ; Hučko and Faria, 1997 ; Meguid et al., 2002 ; Kenesei et al., 2004) have taken into account the properties approximated by precursor material rather than actual cell wall because (i) the geometry of thin cell wall is not suitable enough for making conventional compressive or tensile test specimen, or (ii) in case of conventional tests on foam specimens even at very small loads, local yielding and bending of cell wall take place which make the isolation of elastic and plastic properties almost impossible. These difficulties can be overcome if the load-displacement curve is obtained in a few micron ranges so that load is small enough not to cause cell wall bending and if the initial portion of unloading is used instead of loading curve to assess the elastic properties. This concept can be practically realized by the instrumented nanoindentation technique.

The current study was initiated with the objective to construct the constitutive relation between stress and strain for thin cell wall material by extracting the material parameters through instrumented sharp indentation. The reverse algorithm using dimensionless functions (Dao et al., 2001) was used to determine material parameters from the load-indentation depth curve. A modified cubic-spherical lattice model based on the obtained material parameters was proposed to analyze the compressive behavior of the Al-alloy
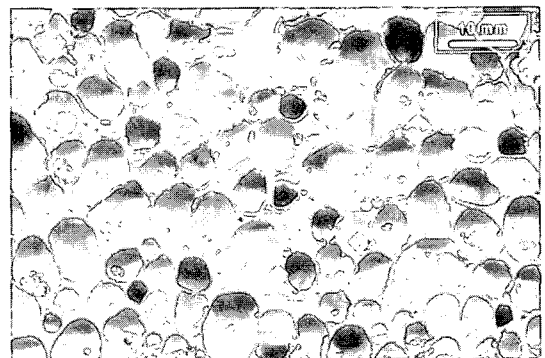
foam.

2. Experimental

2.1 Material and specimen

Al-alloy foam having a composition of Al-3wt.% Si-2wt.%Cu-2wt.%Mg was produced by powder metallurgical method (Kim et al., 2004). To produce the foam precursor, 99%wt.Al alloy powder was mixed with 1%wt.TiH$_2$ particles. The mixture was then consolidated by cold compaction at a pressure of 4 MPa and was hot extruded at a temperature of 430℃ with an extrusion ratio of 20 : 1. Finally the alloy precursor in mould was foamed keeping it in a preheated furnace for foaming time of 10 min at a temperature 700℃. A typical microscopic image of obtained foam is shown in Fig. 1. Specimens of 10 mm thickness were cut from the foam sample as well as the alloy precursor, and were mounted into a thermo-set epoxy resin of 30 mm diameter and 15 mm thickness for nanoindentation test. One face of the mounted specimen was polished to the mirror surface.
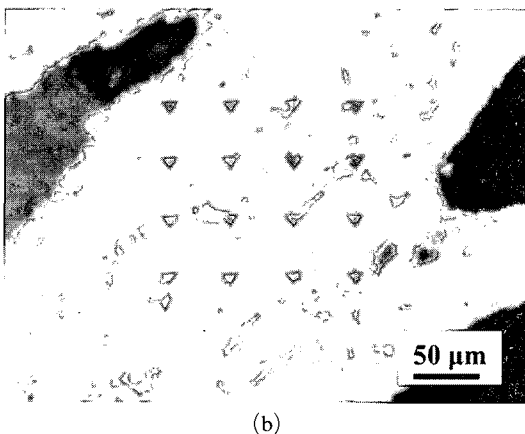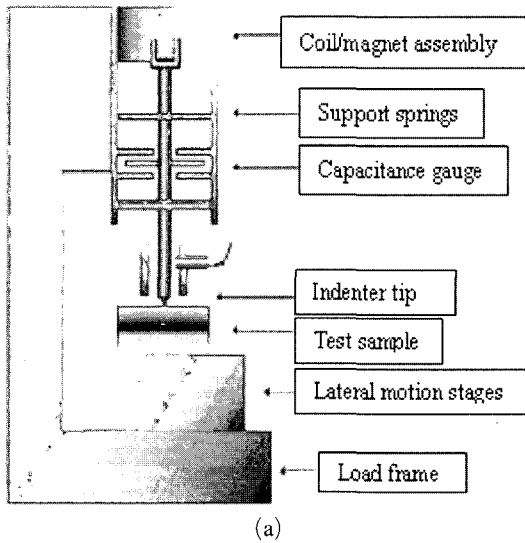
2.2 Experimental setup

Nanoindentation test on cell wall was performed by using MTS nanoindenter XP. Fig. 2(a) depicts a schematic diagram of the experimental setup. The indenter was a Berkovich indenter which is three sided pyramid with an aspect ratio same as that of Vickers indenter. The system had load and displacement resolutions of 50 nN and 0.01 nm respectively. The spots of measurements

Fig. 1   A microscopic view of a typical aluminum alloy foam

were arranged in an array of indentations as shown in Fig. 2(b). It is suggested that the distance between successive indentations should be at least 20 times the maximum penetration depth when using the Berkovich indenter (Nanoindentation XP user manual, Ver. 16). The maximum penetration was 2000 nm, therefore the distance between indentations was kept to be 50 μm. The tensile test specimen was also prepared from the extruded precursor material independently, and tested at a test speed of 1.0 mm/min using an MTS 810 machine.

(a)

(b)

Fig. 2   (a) Schematic diagram of experimental setup for nanoindentation test; (b) indentation marks on the cell wall of Al-Si-Cu-Mg foam

3. Determination of Stress–Strain Relation of Cell Wall Material

The stress–strain relation of Al-alloy can be approximated by a power law with a set of material parameters such as elastic modulus E, strength coefficient K, yield stress σ_y and strain hardening exponent n as shown in Fig. 3. Thus the elasto–plastic true stress–strain behavior is described by the following equation:

$$\sigma = E\varepsilon \text{ for } \sigma \leq \sigma_y$$
$$\sigma = K\varepsilon^n \text{ for } \sigma \geq \sigma_y \tag{1}$$

At the yield point corresponding to initial yield stress σ_y, Eq. (1) becomes as following:

$$\sigma_y = E\varepsilon_y = K\varepsilon_y^n \tag{2}$$

The total strain ε consists of two parts ε_y and ε_p (ε_p is the nonlinear plastic portion of the total strain accumulated beyond ε_y) as following:

$$\varepsilon = \varepsilon_y + \varepsilon_p \tag{3}$$

Substituting Eqs. (2) and (3) for Eq. (1) for $\sigma \geq \sigma_y$ allows one to obtain the following equation:

$$\sigma = \sigma_y \left(1 + \frac{E}{\sigma_y}\varepsilon_p\right)^n \tag{4}$$

Thus an elasto–plastic behavior of material is fully estimated by parameters E, σ_y, n and Poisson's ratio v which must be determined by the load–indentation depth curve shown in Fig. 4.
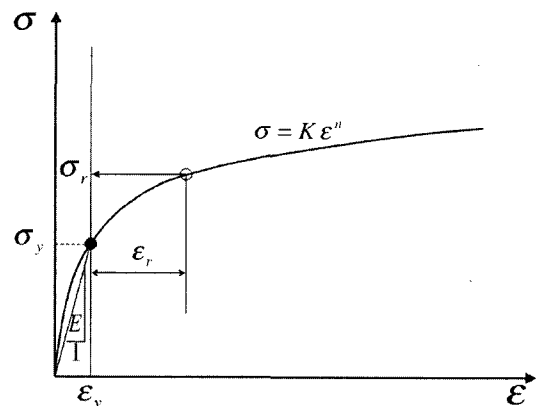
Fig. 3   Power law elasto–plastic stress–strain relation

The load-indentation depth curve behavior during loading can be described by Kick's law as following :

$$P = Ch^2 \qquad (5)$$

Here C is the loading curvature. The hardness of the material is $H_{ave} = \dfrac{P_m}{A_m}$ (A_m is the projected contact area measured at maximum load P_m). The initial unloading slope at h_m is defined as $\dfrac{dP_u}{dh}\Big|_{h_m}$, where P_u is the unloading load. C and $\dfrac{dP_u}{dh}\Big|_{h_m}$ are two independent quantities that can be directly obtained from the load-indentation depth curve.

For a sharp indenter indenting normally into a power law elasto-plastic solid, the load P can be described as following (Dao et al., 2001):

$$P = P(h, E^*, n, \sigma_r) \qquad (6)$$

where E^* is the effective elastic modulus of the indenter specimen system and is defined as following (Dao et al., 2001 ; King, 1987):

$$E^* = \left[\frac{1-\upsilon^2}{E} + \frac{1-\upsilon_{in}^2}{E_{in}}\right]^{-1} = \frac{1}{c^* \sqrt{A_m}} \frac{dP_u}{dh}\Big|_{h_m} \qquad (7)$$

Here E and E_{in} are the elastic moduli of indented and indenter materials respectively. c^* is a constant (1.2370 for large deformation elasto-plastic solution for Berkovich indenter (Dao et al., 2001)),

$P = Ch^2$
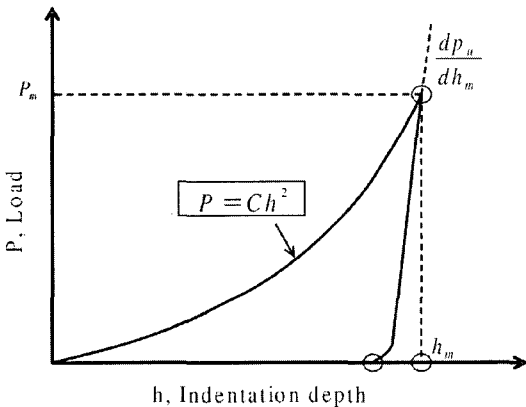
Fig. 4 Schematic diagram of typical load-indentation depth curve of elasto-plastic material by nanoindentation

and A_m is the projected contact area measured at maximum load P_m ($24.56h_m^2$ for Berkovich indenter). Most of the indenter tips are not ideally sharp but rounded to some extent at the apex. A Berkovich tip indenter has a tip radius in the range of 10 nm ~ 100 nm. Thus if indentation is made in the depth close to this range, the behavior of the indentation is affected by the indenter tip rounding. However the tip rounding effect is insignificant and can be ignored for a depth deeper than 1000 nm (Dao et al., 2001 ; Kunert, 2004). In this study the tip rounding effect was ignored as the indentation depth was 2000 nm.

Applying Π theorem in the dimensional analysis, Eq. (6) yields the following :

$$P = \sigma_r h^2 \Pi_1 \left(\frac{E^*}{\sigma_r}, n\right) \qquad (8)$$

Thus the loading curvature C normalized by σ_r may alternatively be expressed as following :

$$\frac{P}{h^2} \frac{1}{\sigma_r} = \frac{C}{\sigma_r} = \Pi_1 \left(\frac{E^*}{\sigma_r}, n\right) \qquad (9)$$

From Eq. (9) it is clear that for an isotropic and homogeneous material $P = Ch^2$ is the natural outcome of the dimensional analysis for a sharp indenter and loading curvature C can be called a material characteristics constant which is independent of indentation depth. The parameter σ_r can be any plastic stress known as the representative stress corresponding to a plastic strain ε_r known as representative strain (Fig. 3). However, the representative strain should be a unique value which best normalizes the particular dimensionless functions with respect to strain hardening. It is so called representative because for its specific value Eq. (9) will give the same functional value of Π_1 irrespective of different values of n. In other words specific functional form of Π_1 independent of strain hardening exponent n depends on the choice of ε_r and σ_r. In this study $\varepsilon_r = 0.033$ was selected as previously used by Dao et al. (2001). In their work, seventy six different combinations of elasto-plastic material parameters such as σ_y, E, n (with four different values of $n = 0$, 0.1, 0.3, 0.5) covering a wide range of parameters commonly found in pure and alloyed engineering materials were fitted to Eq. (9) for three different

values of ε_r (ε_r=0.01, 0.033 and 0.29). Extensive computational study of depth sensing indentation was carried out with those 76 different cases as input material properties, and loading curvature C was evaluated for each case from the load-indentation depth curve. The fittings to Eq. (9) for the aforementioned n values showed the best agreement for Π_1 in case of ε_r=0.033 with a relative error of $\pm 2.85\%$. The corresponding dimensionless function Π_1 normalized with respect to $\sigma_{0.033}$ was found to be independent of strain hardening exponent n and is expressed as follows:

$$\frac{C}{\sigma_{0.033}}=\Pi_1\left(\frac{E^*}{\sigma_{0.033}}\right) \tag{10}$$

On the other hand, the unloading slope $\dfrac{dP_u}{dh}$ can be expressed as following function:

$$\frac{dP_u}{dh}=\frac{dP_u}{dh}(h,\ h_m,\ E^*,\ \sigma_r,\ n) \tag{11}$$

The dimensional analysis of Eq. (11) at $h=h_m$ yields the following:

$$\begin{aligned}\left.\frac{dP_u}{dh}\right|_{h=h_m}&=E^*h_m\Pi_2\left(1,\ \frac{\sigma_r}{E^*},\ n\right)\\&=E^*h_m\Pi_2\left(\frac{E^*}{\sigma_r},\ n\right)\end{aligned} \tag{12}$$

The dimensionless closed-form functions (Π_1 and Π_2) are listed in the Appendix. The procedure to obtain elasto-plastic properties from a load-indentation depth curve is accomplished by Eq. (6) through Eq. (12). With known values of $C,\ \left.\dfrac{dP_u}{dh}\right|_{h_m}$ and h_m from a load-indentation depth curve and E^* from Eq. (7), σ_r can be evaluated by Eq. (10). Consequently the strain hardening exponent n can be calculated by Eq. (12). Finally known values of σ_r, n and E allow one to obtain the yield stress σ_y by using the following equation:

$$\sigma_{0.033}=\sigma_y\left(1+\frac{E}{\sigma_y}\varepsilon_{0.033}\right)^n \tag{13}$$

4. Result and Discussion

4.1 Stress-strain relations for Al-alloy foam cell wall material

Nonlinear large strain FE code ABAQUS was used for the computation and analysis. A two-di-

mensional axisymmetric semi-infinite model was constructed to simulate the load-indentation depth curve of elasto-plastic solid. Considering axisymmetric properties the three-dimensional indentation induced by Berkovich indenter can be approximated with an axisymmetric two-dimensional model by choosing the apex angle such that the projected area/depth of the two-dimensional cone is same as that for Berkovich indenter (Dao et al., 2001 ; Dejun et al., 1998 ; Chen et al., 2005 ; Lichinchi et al., 1998). It is generally agreed that an axisymmetric model with a cone semi-apical angle α=70.3° gives the same area to depth ratio as a pyramidal Berkovich indenter (Andrews et al., 2001). To simplify the modeling and reduce
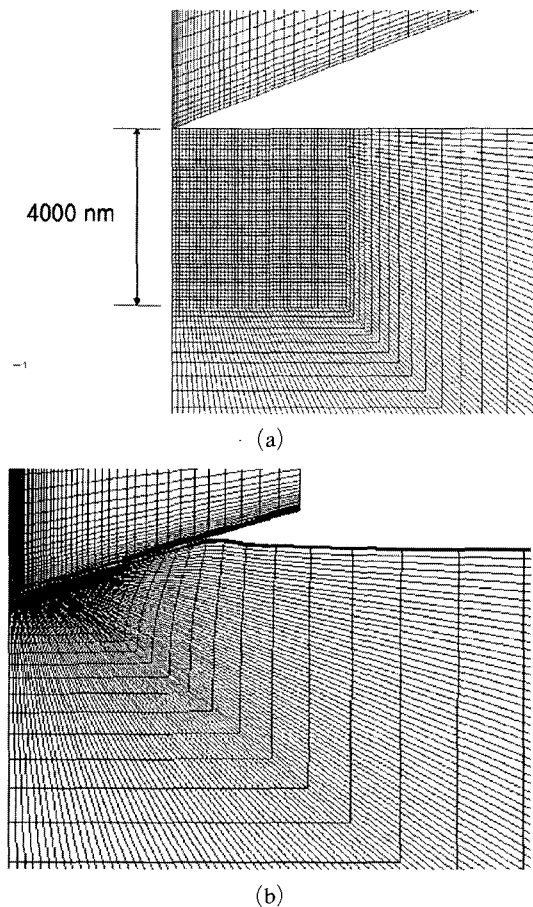

(a)

(b)

Fig. 5 FE model for nanoindentation (a) mesh design for two-dimensional axisymmetric model before indentation ; (b) deformed model after indentation

the execution time, a two dimensional axisymme-
tric model with a semi-angle $\alpha=70.3°$ was con-
structed. Figs. 5(a) and (b) show the meshed
axisymmetric model prior to indentation and after
indentation respectively. A total of 10718 nodes
and 9878 CAX4 elements were used to generate
the model. Fine meshes near the contact region
and gradually coarser meshes farther from the con-
tact region were designed to ensure the numerical
accuracy of large deformation area around the
indenter. The nodes on the bottom were con-
strained in six degrees of freedom. A frictionless
sliding contact was used between indenter and
specimen surface because the friction coefficient
is 0.05~0.15 in which the effect of friction is
negligible (Dao et al., 2001 ; Dejun et al., 1998 ;
Lichinchi et al., 1998). In FE analysis the maxi-
mum penetration depth was 2000 nm same as in
the experiment. The elastic modulus and Poisson's
ratio for the diamond indenter were $E_i=1141$ GPa
and $v_i=0.07$ respectively. The stress-strain rela-
tions extracted from the experimental load-inden-
tation depth curves were used as the input para-
meters for FE simulation.

The material parameters extracted from five in-
dividual experimental load-indentation depth cur-
ves for each of the Al-alloy precursor and foam
cell wall are shown in Table 1. Fig. 6 shows the
stress-strain power law (Eq. (1)) calculated with
extracted average material parameters and the ten-
sile test result for the precursor. Fig. 7 shows the
experimental load-indentation depth curves with
that obtained from FE simulation using the ob-
tained stress-strain relation shown in Fig. 6. The
load-indentation depth curves for Al-alloy pre-
cursor were scattered, which might be caused by
the micro-structural heterogeneity of precursor.
However, the simulation result is in the scatter
range of experimental result.

On the other hand, the experimental and FE
simulated load-indentation depth curves for the
Al-alloy foam cell wall are shown in Fig. 8. The
simulation was carried out with average material
parameters in Table 1. A reasonable agreement
between the experimental and the simulated cur-
ves is apparent in the figure. However, Fig. 9
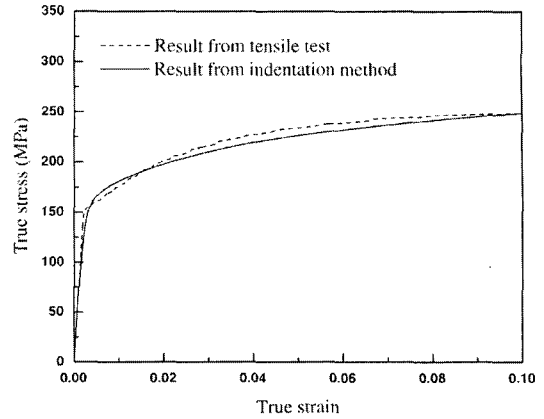reveals that the stress-strain relation of cell wall

Fig. 6 Comparison between stress-strain curves by
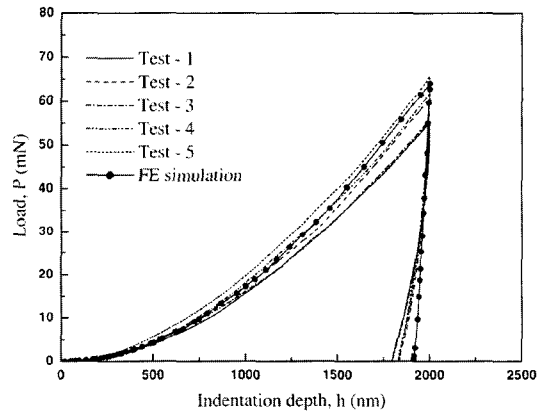tensile test and indentation method for Al-
Si-Cu-Mg precursor

Fig. 7 Experimental and FE load-indentation depth
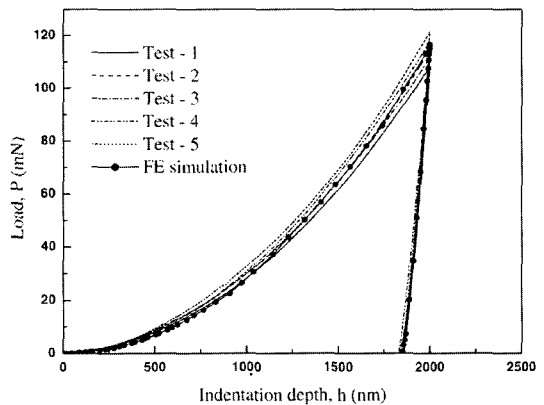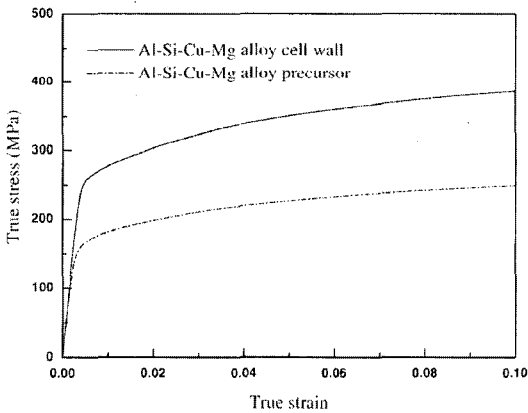curves for Al-Si-Cu-Mg precursor

Fig. 8 Experimental and FE load-indentation depth
curves for Al-Si-Cu-Mg foam cell wall

Table 1 Material parameters for Al–Si–Cu–Mg precursor and foam cell wall

	Test No.	Elastic modulus, E (GPa)	Strain hardening exponent, n	Yield stress, σ_y (MPa)
Al–Si–Cu–Mg precursor material	Test-1	65.63	0.155	132
	Test-2	67.00	0.113	170
	Test-3	76.36	0.130	159
	Test-4	66.43	0.149	133
	Test-5	75.19	0.107	154
	Average	70.12	0.131	150
Al–Si–Cu–Mg foam cell wall	Test-1	72.22	0.128	235
	Test-2	71.23	0.139	248
	Test-3	60.91	0.121	253
	Test-4	69.34	0.135	263
	Test-5	76.58	0.180	211
	Average	70.06	0.140	242

Fig. 9 Stress–strain relations for Al–Si–Cu–Mg foam cell wall and precursor

(a)　　　　　　　　　(b)

Fig. 10 FE model of foam (a) before deformation ; (b) after deformation

is very different from that of the precursor, indicating that the manufacturing process such as foaming, heat treatment and cold works influenced the stress–strain ·relation of the cell wall material.

4.2 FE model for the compressive behavior analysis of Al-alloy foam

The extracted stress–strain relation can be utilized to evaluate compressive property of Al-alloy foam. A modified cubic–spherical lattice FE model for closed cell Al-alloy foam was proposed in this study as shown in Fig. 10. The basic buil-
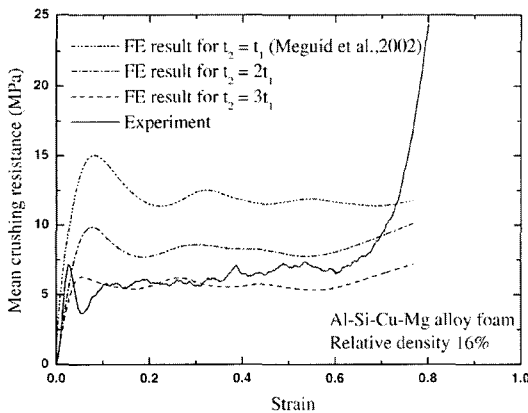
ding block of the FE model was taken similar to a truncated cube model (Santosa and Wierzbicki, 1998) which was composed of cruciform and pyramidal sections. In order to imitate the structure of real closed cell foam, the different thicknesses were implemented to the cruciform (t_1) and spherical (t_2) cell walls in this study. The ratio of diameter (D) of the spherical cell to width (W) of the cruciform section was assumed as 0.5. The

cell thicknesses with a ratio $\left(\dfrac{t_2}{t_1}\right)$ were determined from the relationship between the relative density of foam and the volume fraction of the skeleton in the model (Kim et al., 2005).

In the FE analysis, the average material parameters for Al-alloy foam cell wall shown in Table 1 were used, where $\sigma_y=242$ MPa, $E=72.06$ GPa and $n=0.140$. The simulation was carried out by using nonlinear explicit FE code LS-DYNA 3D. The four noded Belytschko-Tsay Lin shell element with six degrees of freedom per node (three translations and three rotations) and self-contact was used. A piecewise linear plastic material in LS-DYNA 3D material library was used. The contact between the upper surface of FE model and the compression plate was automatic surface to surface contact. One translational movement of the top surface was allowed with five degree constraints while six degree constraints were applied to the bottom of the model. Symmetry conditions were applied on all free vertical and horizontal edges. Fig. 11 represents the numerical mean crushing strength behavior of the foam model for various thickness ratios. The mean crushing strength σ_m is defined as following :

$$\sigma_m=\frac{1}{\varepsilon}\int_0^\varepsilon \sigma(\varepsilon)\,d\varepsilon \qquad (14)$$

Here $\sigma(\varepsilon)$ is the instantaneous crushing strength

corresponding to the instantaneous strain ε. The mean crushing strength of model with a thickness ratio of 3 was found to be best matched with the crushing strength of real Al-alloy foam. It has much lower crushing strength than the cruciform-hemisphere model (Meguid et al., 2002).

5. Conclusion

The stress-strain curve of thin cell wall material of Al-alloy foam was determined by an instrumented sharp indentation method. In order to characterize the stress-strain relation, the dimensionless functions proposed by Dao et al. were utilized. The obtained material parameters of cell wall material were found to be very different from those of precursor. The modified cubic-spherical lattice model with a thickness ratio of 3 having the proper material parameters extracted by the nanoindentation method allowed one to obtain the solutions closer to the real compressive behavior of the Al-alloy foam.

Acknowledgments

References

Andrews, E. W., Gioux, G., Onck, P. and Gibson, L. J., 2001, "Size Effects in Ductile Cellular Solids. Part II: Experimental Results," *International Journal of Mechanical Science*, Vol. 43, pp. 701~713.

Chen, X., Xiang, Y. and Vlassak, J. J., 2005, "A Novel Technique for Measuring the Mechanical Properties of Porous Materials by Nanoindentation," *Journal of Materials Research*, In press.

Dao, M., Chollacoop, N., Van Vliet, K. J., Venkatesh, A. and Suresh, S., 2001, "Computational Modeling of the Forward and Reverse

Fig. 11 Compressive crushing resistance for Al-Si-Cu-Mg foam obtained from experiment and FE simulation with various thickness ratios

Problems in Instrumented Sharp Indentation," *Acta Materialia*, Vol. 49, pp. 3899~3918.

Dejun, M., Kewei, X. and Jiawen, H., 1994, "Numerical Simulation for Determining the Mechanical Properties of Thin Metal Films Using Depth-Sensing Indentation Technique," *Thin Solid Films*, Vol. 323, pp. 183~187.

Hučko, B. and Faria, L., 1997, "Material Model of Metallic Cellular Solids," *Computers & Structures*, Vol. 62, No. 6, pp. 1049~1057.

Kenesei, P., Kádár, C., Rajkovits, Zs. and Lendvai, J., 2004, "The Influence of Cell Size Distribution on the Plastic Deformation in Metal Foams," *Scripta Materialia*, Vol. 50, pp. 295~300.

Kim, A., Cho, S. S. and Lee, H. J., 2004, "Foaming Behavior of Al-Si-Cu-Mg Alloys," *Materials Science and Technology*, Vol. 20, pp. 1615~1620.

Kim, A., Tunvir, K., Park, S. J., Jeong, G. D., Hasan, M. A. and Cheon, S. S., 2005, "Study on Compressive Behavior of Heterogeneous Al-alloy Foam by Cruciform-Hemisphere Model," *Proc. KSME 2005 Spring Conference*, pp. 500~505.

King, R. B., 1987, "Elastic Analysis of Some Punch Problems for a Layered Medium," *International Journal of Solids Structure*, Vol. 23, pp. 1657~1664.

Kunert, M., 2000, "Mechanical Properties on Nanometer Scale and Their Relations to Composition and Microstructure-A Nanoindentation Study on Carbon Implanted Ti-Al-4V," Ph. D.

Dissertation, Max-Planck-Institute for Metallforschung, Stuttgart.

Lichinchi, M., Lenardi, C., Haupt, J. and Vitaly, R., 1998, "Simulation of Berkovich Nanoindentation Experiments on Thin Films Using Finite Element Method," *Thin Solid Films*, Vol. 312, pp. 240~248.

Meguid, S. A., Cheon, S. S. and Abbasi, N. EI., 2002, "FE Modeling of Deformation Localization in Metallic Foams," *Finite Elements in Analysis and Design*, Vol. 38, pp. 631~643.

Nanoindentation XP User's manual (version. 16). Test Works 4 Software pp. 32~34.

Overaker, D. W., Cuitino, A. M. and Langrana, N. A., 1998, "Effects of Morphology and Orientation on the Behavior of Two Dimensional Hexagonal Foams and Application in a Re-entrant Foam Anchor Model," *Mechanics of Materials*, Vol. 29, pp. 43~52.

Santosa, S. and Wierzbicki, T., 1998, "On the Modeling of Crush Behavior of a Closed Cell Aluminum Foam Structure," *Journal of the Mechanics and Physics of solids*, Vol. 46, pp. 645~669.

Simone, A. E. and Gibson, L. J., 1998, "The Effects of Cell Face Curvature and Corrugations on the Stiffness and Strength of Metallic Foams," *Acta Mater*, Vol. 46, pp. 3929~3935.

Tabor, D., 1951, *Hardness of metals*, Clarendon Press, Oxford, UK (1951).

Appendix

$$\Pi_1 = \frac{C}{\sigma_{0.033}} = -1.131\left[\ln\left(\frac{E^*}{\sigma_{0.033}}\right)\right]^3 + 13.635\left[\ln\left(\frac{E^*}{\sigma_{0.033}}\right)\right]^2 - 30.594\left[\ln\left(\frac{E^*}{\sigma_{0.033}}\right)\right] + 29.267$$

$$\Pi_2\left(\frac{E^*}{\sigma_r},\ n\right) = \frac{1}{E^* h_m}\frac{dP_u}{dh}\bigg|_{h_m} = (-1.40557n^3 + 0.77526n^2 + 0.15830n - 0.06831)\left[\ln\left(\frac{E^*}{\sigma_{0.033}}\right)\right]^3$$

$$+ (17.93006n^3 - 9.22091n^2 - 2.37733n + 0.86295)\left[\ln\left(\frac{E^*}{\sigma_{0.033}}\right)\right]^2$$

$$+ (-79.99715n^3 + 40.55260n^2 + 9.00157n - 2.54543)\left[\ln\left(\frac{E^*}{\sigma_{0.033}}\right)\right]$$

$$+ (122.65069n^3 - 63.88418n^2 - 9.58936n + 6.20045)$$